frontiers | Frontiers in Earth Science

TYPE Original Research
PUBLISHED 15 September 2022
DOI 10.3389/feart.2022.1018465

OPEN ACCESS

EDITED BY
Mingjun Zou,
North China University of Water Resources and Electric Power, China

REVIEWED BY
Gaoyuan Yan,
China University of Mining and Technology, China
Yu Qi,
Yanshan University, China

*CORRESPONDENCE
Keying Wang,
744491522@qq.com

SPECIALTY SECTION
This article was submitted to Economic Geology, a section of the journal Frontiers in Earth Science

RECEIVED 13 August 2022
ACCEPTED 26 August 2022
PUBLISHED 15 September 2022

CITATION
Cai N, Wang K and Du J (2022), Geological occurrence and productivity prediction for coalbed methane of central Hunan depression, China. *Front. Earth Sci.* 10:1018465. doi: 10.3389/feart.2022.1018465

Geological occurrence and productivity prediction for coalbed methane of central Hunan depression, China

Ningbo Cai[1,2,3], Keying Wang[2,3]* and Jiang Du[2,3]

[1]Institute of Advanced Studies, China University of Geosciences, Wuhan, China, [2]New Geological Energy Exploration and Development Engineering Technology Research Center of Hunan, Changsha, China, [3]Geophysics and Geochemistry Survey Institute of Hunan, Changsha, China

To analyze the geological occurrence and predict the drainage performance of coalbed methane in the central Hunan depression of China, coal samples were collected to conduct physical experiments and numerical simulations. The following conclusions were reached. The vitrinite ranges from 54.37 to 87.80%, the inertinite is between 11.14–25.89%, and exinite is less than 1%. The inorganic components are mainly clay minerals and vary from 0.71 to 5.66%. The major porosity ranges from 7 to 9%, and it is influenced by organic/inorganic components and maturity. Both the vertical and horizontal permeabilities are at a relatively low level, mostly below 0.05 mD, indicating the reservoir is low permeable or non-permeable. The reservoir pressure ranges from 3.74 to 11.58 MPa, which has significant and positive linear correlations with closure pressure and burial depth. Gas content varies from 5 m^3/t to 20 m^3/t. The theoretical recovery ratio in the Hongshandian mining area is about 61.7%, while the values of the two spots in the Duanpiqiao mining area are 49.1 and 54.5%. Production predictions show that under the permeability of 0.01 mD, 0.05 mD, and 0.10 mD, cumulative gas productions in 10 years for a single well range from 1.7×10^6 m^3 to 3.2×10^6 m^3, and those for a well group consisting of five wells vary from 10.5×10^6 m^3 to 19.2×10^6 m^3. Thus, this area will have a high value for coalbed methane exploitation after stimulating the reservoir to increase permeability successfully.

KEYWORDS

coalbed methane, geological occurrence, productivity prediction, longtan formation, central hunan depression

1 Introduction

Since the 1990s, unconventional gas explorations have made breakthroughs in America, Canada, and other countries (Schmoker, 1980; Law, 2002a; Law, 2002b; Curtis, 2002). Foreseeing its importance, Chinese geologists (Huang, 1990) proposed using coal measure gas. As one type of coal measure gases, coalbed methane (CBM) is potentially an important and abundant economic resource that has received worldwide

TABLE 1 Basic information of coal mines and samples.

Mining area	Mining area abbreviation	Location	Geological time	Coal type	$R_{o,max}$/%
Zhadu	ZD	Central of Hunan Depression	P_3l	Anthracite	2.80
Lengshuijiang	LSJ		P_3l	Anthracite	2.78
Lumaojiang	LMJ		P_3l	Anthracite	2.68
Hongshandian	HSD		P_3l	Meager coal	2.05
Duanpoqiao	DPQ		P_3l	Lean coal	1.64
Doulishan	DLS		P_3l	Coking coal	1.23
Gujiaodi	GJD		P_3l	Lean coal	1.68
Meitanba	MTB		P_3l	Fat coal	1.05
Yonglei	YL	Southeastern Hunan Depression	P_3l	Anthracite	2.87
Taoshui	TS		P_3l	Anthracite	2.80
Matian	MaT		P_3l	Anthracite	2.29
Baisha	BS		P_3l	Anthracite	2.87
Meitian	MeiT		P_3l	Anthracite	2.89
Yuanjia	YJ		P_3l	Anthracite	2.91

Geological time: P_3l= Longtan formation of upper series Permian System

attention in recent years (Bustin and Clarkson, 1998; Wei and Zhang, 2010; Liu et al., 2013; Sun et al., 2016; Liu and Wu, 2017).

The geological and geochemical characteristics of unconventional gas-bearing systems, including CBM reservoirs, were discussed in Martini et al. (2003). With further research on unconventional gas, scholars made in-depth studies on accumulation mechanism, occurrence conditions, and exploration, development, and utilization models of unconventional gas resources in sedimentary basins, especially for CBM resources (Laubach and Gale, 2006; Liu et al., 2013; Zou et al., 2013; Liu and Wu, 2017; Qin, 2018; Zou et al., 2018; Tao et al., 2019). A consensus has been reached that it is crucial to further understand the coal reservoir features and predict recoverability performance (Wang et al., 2009; Wei et al., 2010; Zhang, 2014; Zhang and Bian, 2015). This understanding can be the basis for both delineating a target exploitation area and designing a reasonable drainage system (Wei et al., 2007).

CBM exploration and exploitation in the Hunan province has been carried out for nearly six decades. Although industrial levels of CBM flow have yet to be found, there are multiple sets of high-quality hydrocarbon source rocks in various types, multiple combinations of gas generative stratum, reservoir and cap strata, and diverse types of hydrocarbon-bearing basins in the central Hunan depression. In addition, the developed and widespread distributed coal seams of the Longtan formation in the Permian system provide a physical basis for forming unconventional gas reservoirs. The geological setting for CBM formation is extensively studied in this area (Zou et al., 2015; Zou et al., 2019; Li et al., 2020). Thus, it is of great theoretical significance to investigate the geological occurrence and production prediction of CBM resources of the Longtan formation in the central Hunan depression to guide CBM exploitation.

2 Samples and experiments

2.1 Sample collection and preparation

Coal samples were collected from the Longtan formation in different mining areas of the central Hunan depression, with a size of 30 cm × 30 cm × 15 cm. For comparison purposes, coal samples from some mining areas in the southeast Hunan depression were also collected. The samples were shipped back to the laboratory immediately after collection. Following China's national standard of GB/T 16773-2008, small pieces of samples were selected, ground to 30 mesh, and formed into pulverized coal light sheets. Then, following China's national standard of GB/T6948-1998, the reflectance of oil-impregnated vitrinite of each sample was measured with a ZEISS Imager.M1m microscopic spectrophotometer. A series of coal samples were prepared based on the maximum reflectance data, which are shown in Table 1, and the perspective locations of mining areas can be found in Figure 1.

Three types of samples were prepared for this study. The first type was cylinder samples with a diameter of 25 mm and a height of 30–50 mm; they were used for the permeability test. The second type was block samples with a maximum length of about 15 mm, which were used for the mercury intrusion porosimetry and the isothermal adsorption measurement. The last type was particle samples of about 3 g weight and 60 mesh in size, and they

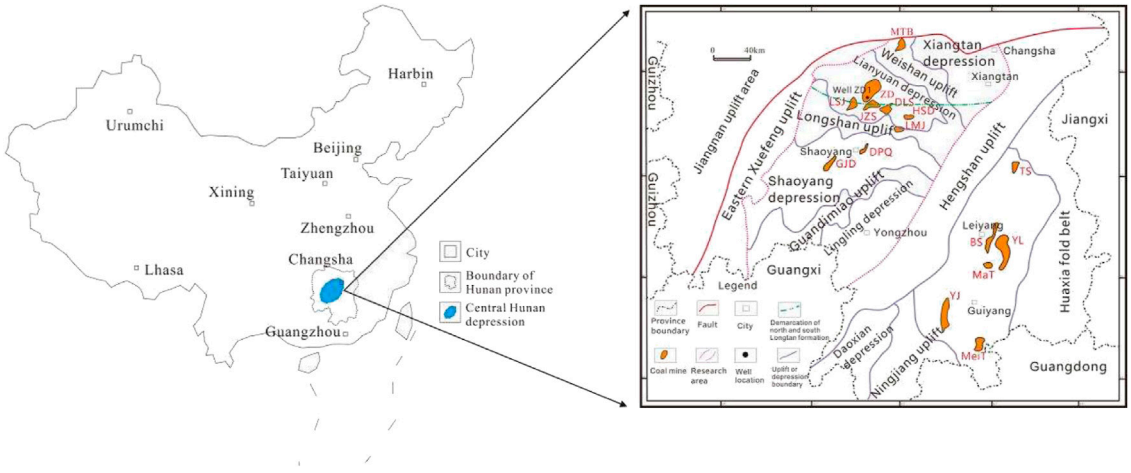

FIGURE 1
Structure outline map of central Hunan depression and distribution of mining areas.

were prepared for the scanning electron microscope analysis and the maceral component measurement.

2.2 Experimental method

The above-mentioned experiments were performed on the prepared coal samples, and gas component analysis was conducted on the gas sample collected from the CBM well. Well-testing analysis and gas content measurement were also made on the mine site.

Maceral component measurement was used to analyze the organic/inorganic compositions following the Chinese oil and gas industry standard (SY/T) 5125-2014 and 5163-2010. Scanning electron microscope analysis was used to analyze pore type and microfracture development following China's national standard of GB/T 25189-2010. Mercury intrusion porosimetry and permeability test were used to measure porosity and permeability, respectively. The mercury intrusion porosimetry measurement ran to a pressure of 6×10^4 Psia and showed that pore diameters as small as 3 nm were penetrated. The permeability test was simulated under situ stress conditions using a triaxial cell with an isotropic ambient pressure of 2.5 MPa. The isothermal adsorption measurement was used to analyze the isothermal adsorption characteristics of the samples to obtain Langmuir volume and pressure. The Langmuir equation and capacity method were adopted during the measurement with a temperature of 30 °C. The gas component analysis measured gas components, including heavy hydrocarbon content. The gas chromatography method was used in this analysis, following China's national standard of GB/T 13610-92. The gas content was measured using the desorption method, and the gas content consisted of desorbed gas, residual gas, and lost gas. The well testing analysis measured reservoir pressure and closure pressure using a common pressure build-up test.

3 Geological setting

The central Hunan depression of China is the area of research addressed in this paper. The Zhadu, Lengshuijiang, Doulishan, Hongshandian, Duanpoqiao, and Gujiaodi mining areas are located inside this depression. The Baisha, Taoshui, and Matian mining areas are distributed in the surrounding areas. The Lianyuan coal-bearing area is in the northern research area, and the main structure inside is the Lianyuan depression, in which a series of broad and gentle short synclines are distributed from west to east. In addition, the Weishan uplift and Xiangtan depression exist in the northern part of the Lianyuan depression. The Shaoyang coal-bearing area is in the center of the research area, in which the main structure is the Shaoyang depression, where there is a series of synclines of closed type or spreading type from west to east. The Lingling depression is in the south of the research area with a complex structure. It consists of a series of closed folds trending northwest and thrust faults trending northeast, which often form imbricate structures and are associated with lateral faults. The structure distribution is shown in Figure 1.

There are three coal-bearing strata in the research area: the Ceshui formation of the lower series Carboniferous system (C_1c), the Longtan formation of the upper series Permian system (P_3l) (south type and north type), and the Lower Jurassic (J_1). The Longtan formation of the upper series Permian system (P_3l) is the main coal-bearing stratum in the area, and it is the target stratum in this study. According to the contact relationship between

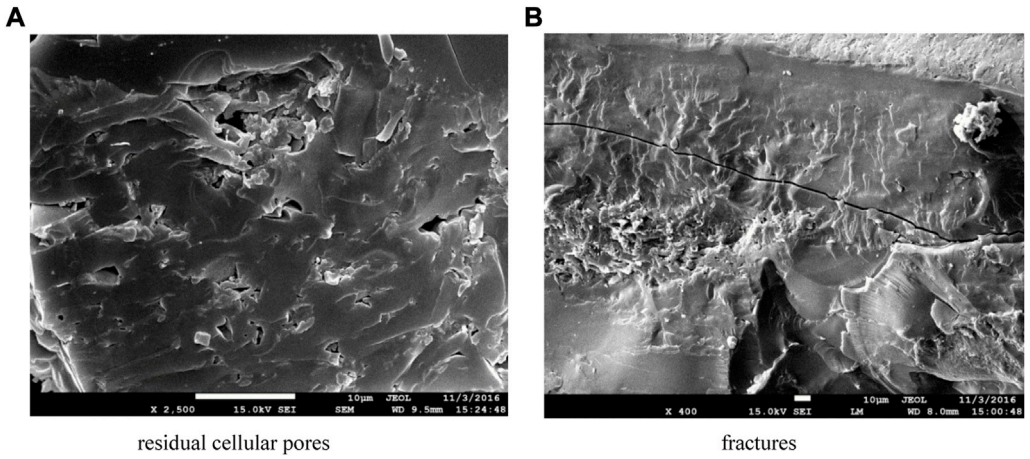

FIGURE 2
Microscopic characteristics of pores and fractures.

upper and lower strata, roughly bounded by 27°40′ N latitude, the Longtan formation in the research area is divided into northern and southern subtypes. The Longtan northern type has a thin thickness and a small quantity of coal seam layers. It is composed of sandstone, siltstone, sandy mudstone, carbonaceous mudstone, and coal seam. The thickness of the minable coal seam is 0.7–3.2 m. The Longtan south type is fully developed and has a large thickness, which can be divided into upper and lower sections. There is no coal seam in its lower section. Its upper section always contains 5–10 layers of coal seams, among which there are two extractable coal seams with a cumulative thickness of 0–12.50 m.

4 Reservoir property and recoverability evaluation

4.1 Coal petrography

Coal seams are generally light black to black or steel gray in color and possess a glassy, strong glassy, and semi-metallic to metallic luster. They have uniform block, granulose, striped, and scaly structures. Most have fractures inside. The fractures present a jagged shape or ladder pattern, graininess, and are partially conchoid. The coal type in the north type of the Longtan formation is usually semi-bright to semi-dark coal, and the bright coal is scant. In the south type of Longtan formation, most of the coal is semi-bright to bright, and the semi-dark and dark coal is scant. Maceral component measurement indicates that the vitrinite is 54.37–87.80%, the inertinite is 11.14–25.89%, the exinite is 0.35–14.08% with mostly lower than 1%, and the inorganic component is 0.71–5.66% of the total. The inorganic component is mainly clay mineral.

4.2 Pore and fracture systems

4.2.1 Pore type and porosity

Coal in the study area develops residual cellular pores and stomas, and fractures can also be detected. The primary structure of the coal body is mainly complete, as shown in Figures 2A,B.

Mercury intrusion porosimetry was conducted to obtain the porosity of coal samples in Table 1. Note that more than one sample was collected and tested in some coal areas, such as the Taoshui (TS) and Baisha (BS) coal areas. The number of tested coal samples is 17, and the results are shown in Figure 3.

The porosity ranges from 6.59 to 15.94%, mostly between 7–9%, placing it in the medium to high porosity reservoir. Scatter diagrams of vitrinite content, inertinite content, inorganic content and maximum vitrinite reflectance versus porosity are presented in Figure 4. Porosity is negatively correlated with vitrinite content and positively correlated with inertinite content. Vitrinite mainly develops micropores that result in a porosity reduction, and inertinite usually develops macropores that result in a porosity increase. Porosity is negatively correlated with the inorganic component. The porosity decreases as the inorganic component increases because the clay minerals fill the coal pores. Porosity is positively correlated with maximum vitrinite reflectance.

4.2.2 Fracture features

Scanning electron microscope analysis of the samples from the Hongshandian mining area shows that microfractures in this area are well developed. The fracture density is 19–35 strip/5 cm, as shown in Figure 5. The microfracture characteristics of the samples from other mining areas in the study area are shown in Figure 6. There is a significant correlation between microfracture density and coal type. The microfracture density decreases from

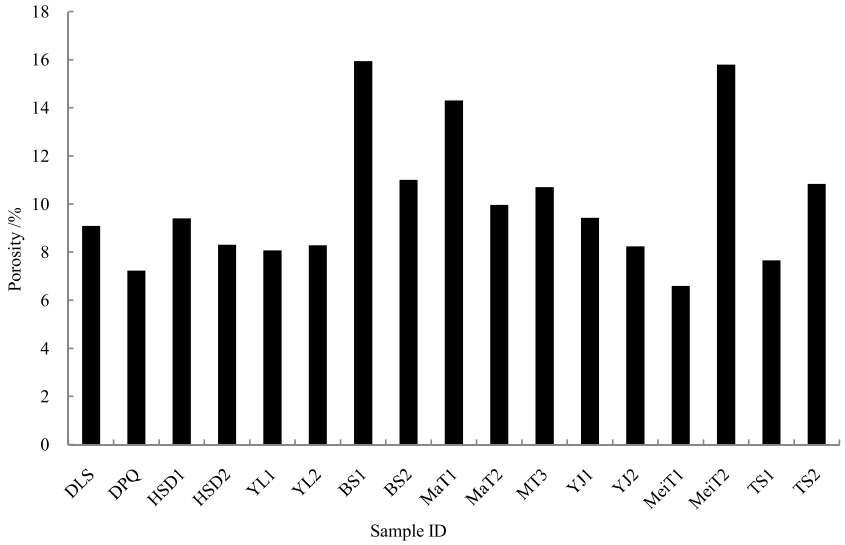

FIGURE 3
Porosity distribution of 17 samples.

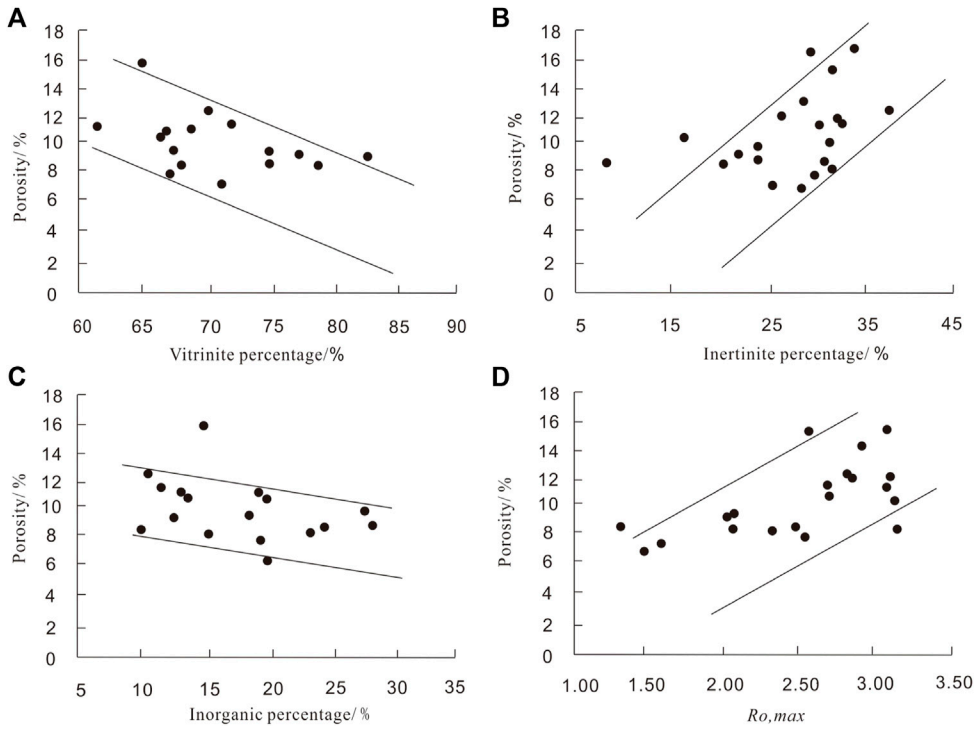

FIGURE 4
Relationships between porosity versus vitrinite **(A)**, inertinite **(B)**, inorganic **(C)**, and maximum vitrinite reflectance **(D)**.

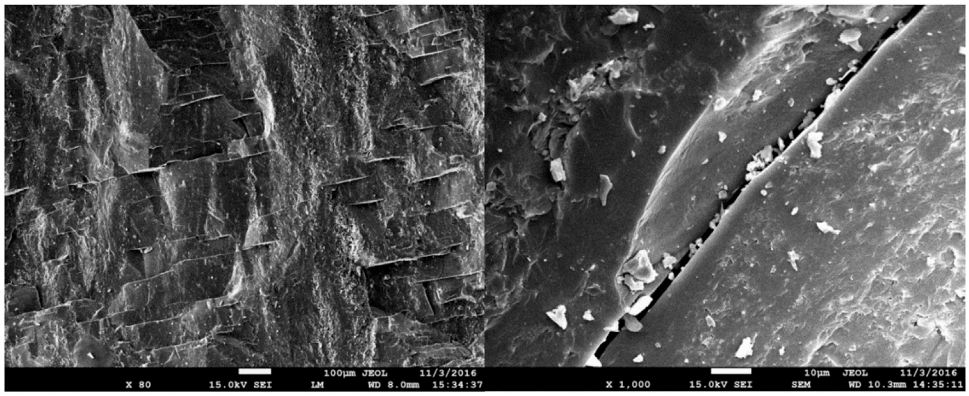

FIGURE 5
Microfractures in the Hongshandian mining area.

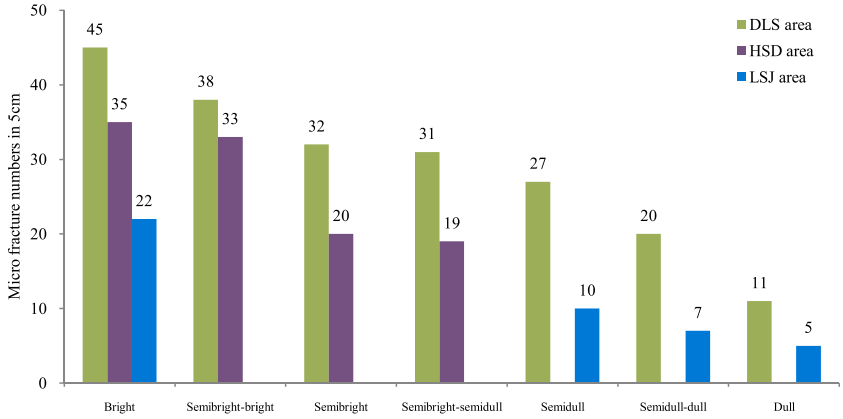

FIGURE 6
Histogram of microfracture density with coal type.

bright coal to dark coal in the same coalification. For example, in the samples from the Doulishan mining area, the microfracture density in xylovitrain is 45 strip/5 cm and decreases to only 11 strip/5 cm in dull coal. The microfracture density in the samples from the Lengshuijiang mining area also significantly decreases from 22 strip/5 cm in bright coal to 5 strip/5 cm in dull coal.

4.2.3 Permeability

Permeability test results are shown in Figure 7. With the deep burial depth and high crustal stress, the vertical permeability is relatively low, in the 0.001–0.025 mD range. Compared with vertical permeability, the horizontal permeability varies between 0.013 mD and 0.082 mD, most of which is lower than 0.05 mD. Thus, the research area is mainly low permeable or non-permeable.

4.3 Reservoir pressure

Reservoir pressure refers to the fluid pressure in coal seam pores, which represents the formation energy. It plays an important role in gas occurrence and CBM drainage. Based on the well testing, reservoir pressure, closure pressure, and corresponding burial depth data were collected in all the mining areas. A scatter diagram and a fitting analysis are shown in Figure 8. The reservoir pressure ranges from 3.74 to 11.58 MPa, which is relatively high. The fitting analysis shows that the reservoir pressure is influenced in linear and positive correlations by closure pressure and burial depth. These results show that the coal seam has higher formation energy, which is beneficial for CBM adsorption and desorption. On the other hand, the higher reservoir pressure might be caused by high

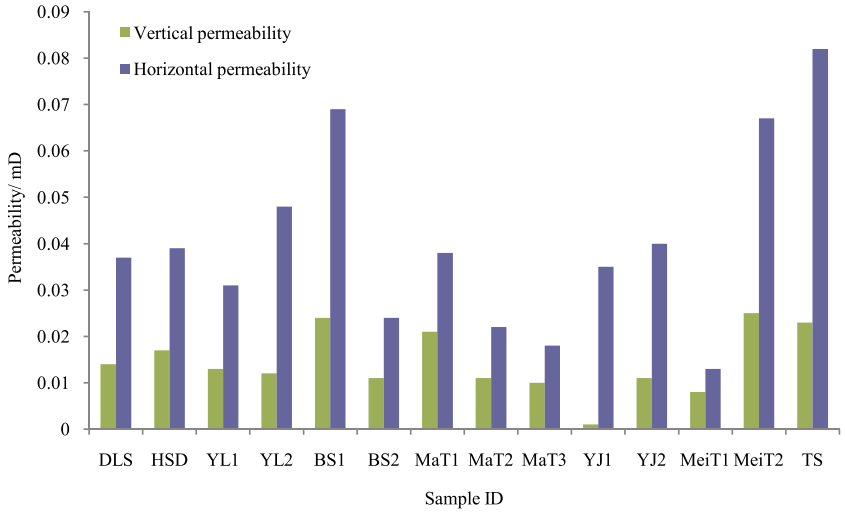

FIGURE 7
Histogram of vertical and horizontal permeability.

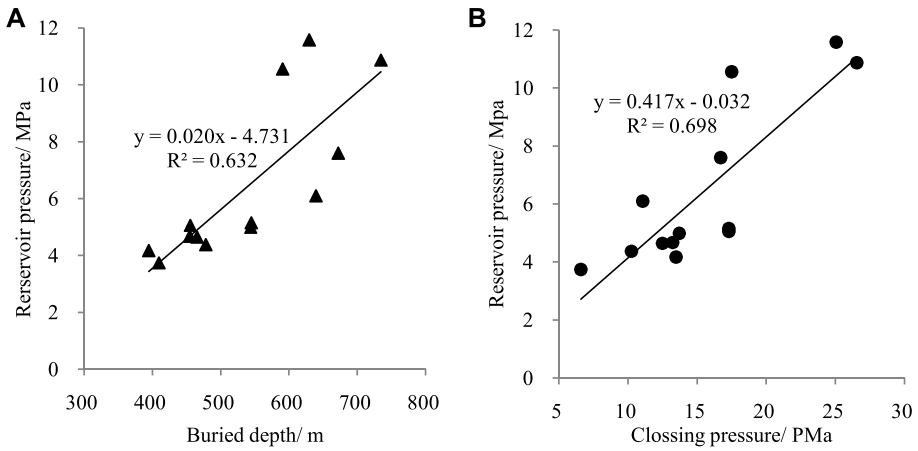

FIGURE 8
Fitting diagram of reservoir pressure versus burial depth **(A)** and crustal stress **(B)**.

crustal stress, often associated with tectonic coal and low permeability, which is unfavorable for CBM exploitation.

4.4 Adsorption characteristics

The isothermal adsorption measurement was conducted, and data pairs of Langmuir volume and pressure were both collected. The Langmuir volume is from 12.43 m^3/t to 33.27 m^3/t and is generally higher than 25 m^3/t. The Langmuir pressure varies from 1.05 to 3.63 Mpa and is mostly higher than 2 MPa. Thus, the overall Langmuir volume is large, indicating that the coal has a strong adsorption capacity. The fitting analyses between Langmuir volume/Langmuir pressure and maximum vitrinite reflectance are shown in Figure 9. This figure shows that a quadratic polynomial relation exists between Langmuir volume and maximum vitrinite reflectance, with a fitting degree of about 0.71. A weak and negative correlation exists between Langmuir pressure and maximum vitrinite reflectance.

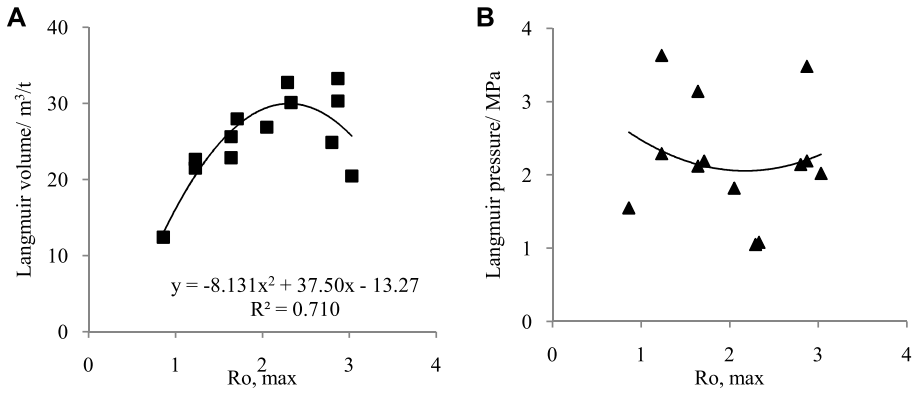

FIGURE 9
Fitting diagram between maximum vitrinite reflectance versus Langmuir volume **(A)** and Langmuir pressure **(B)**.

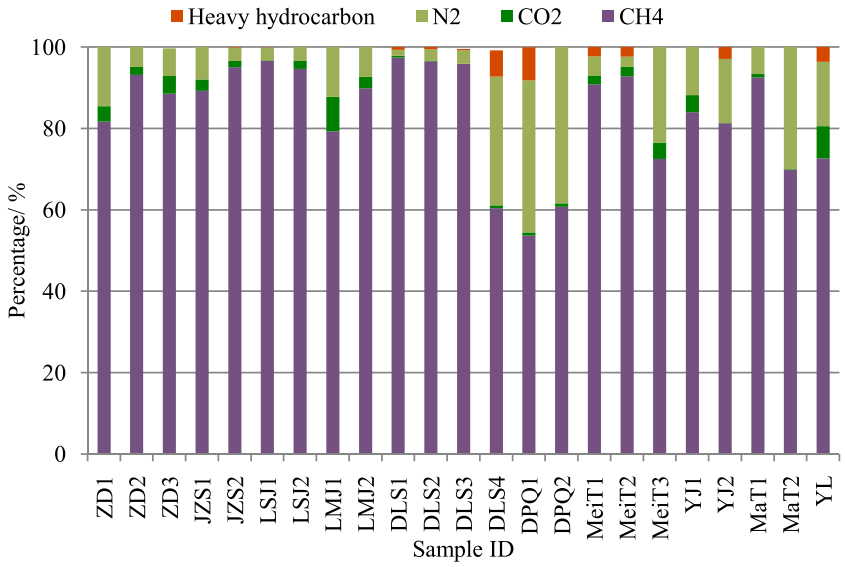

FIGURE 10
Histogram of gas components.

4.5 Gas-bearing characteristics

4.5.1 Gas component analysis

Gas component analysis was conducted for the gas samples, and the results are shown in Figure 10. Methane is the main component, and its percentage ranges from 53.7 to 97.68%, generally higher than 80%. The CO_2 percentage varies between 0.04 and 8.42%, generally higher than 2%. The N_2 percentage is between 1.5–38.4%, and the average is 12.5%. The heavy hydrocarbon percentage is between 0.067–8.11%, with an average of 2.6%.

4.5.2 Gas content

The gas content of 42 points of mining areas in the research area was collected, as shown in Figure 11. The gas content ranges between 2.0 m^3/t and 30.3 m^3/t, and most values are between 5–20 m^3/t. Therefore, CBM is relatively abundant in this area, according to China's national standard of GB/T 29119-2012.

4.6 Recoverability evaluation

Based on isothermal adsorption measurements, the recoverability can be calculated as follows. The gas content under

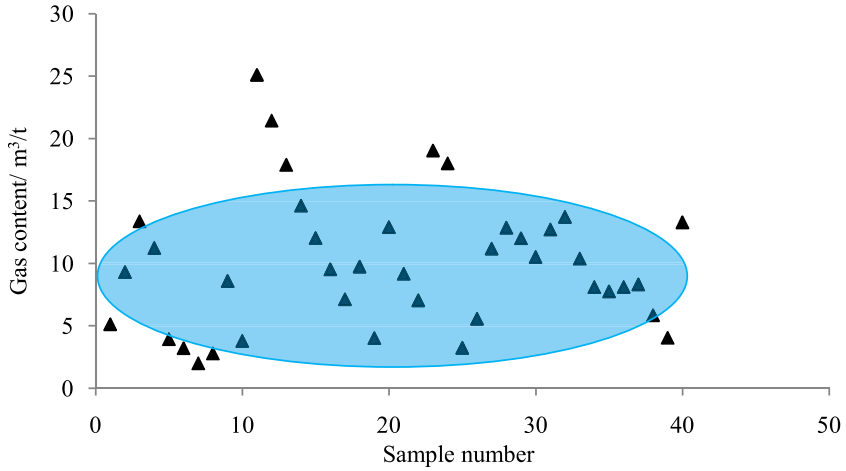

FIGURE 11
Scatter diagram of gas content.

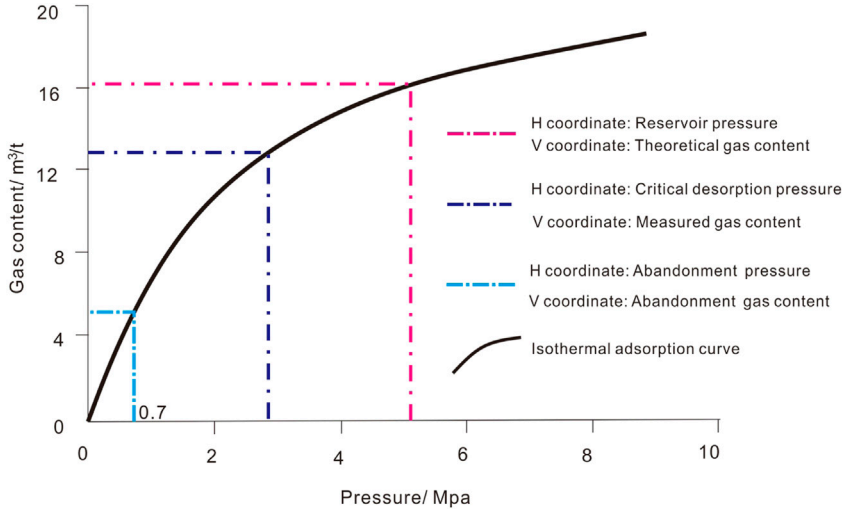

FIGURE 12
Isothermal adsorption curve and its major parameters (H: horizontal; V: vertical).

abandonment pressure (usually 0.7 MPa) can be distinguished by projecting 0.7 MPa to the isothermal adsorption curve, and the recoverability is then calculated using this gas content divided by the measured gas content. The major parameters are shown in Figure 12. Data on three points in Hongshandian and Duanpoqiao mining areas are taken as examples, and calculation results are listed in Table 2. The theoretical recoverability in the Hongshandian mining area is as high as 61.7%, while the values of the two points in the Duanpoqiao mining area are 49.1 and 54.5%. Therefore, the theoretical recoverability is relatively high in this area, indicating a high CBM exploitation value.

5 CBM productivity prediction

A typical CBM well, named well ZD01, in the Zhadu mining area is used as an example. With an assumption of a reasonable drainage system, the CBM productivities of a single well and well

TABLE 2 Recoverability evaluations for mining areas of Hongshandian and Duanpoqiao.

Coal area	HSD	DPQ1	DPQ2
Measured gas content/m^3/t	18.46	11.2	12.87
Reservoir pressure/MPa	4.65	4.43	5.10
Langmuir volume/m^3/t	27.97	22.66	23.05
Langmuir pressure/MPa	2.188	2.15	2.16
Calculated gas saturation/%	66.0	49.3	55.84
Measured gas saturation/%	97.1	73.4	79.5
Critical desorption pressure/MPa	4.25	2.10	2.70
Ratio of critical desorption pressure and reservoir pressure	0.92	0.48	0.54
Calculated recoverability/%	61.7	49.1	54.5

TABLE 3 Reservoir parameters for well ZD01.

Parameter	Value	Source
Buried depth	600 m	Tested
Permeability	0.01; 0.05; 0.1 mD	Set
Porosity	9%	Tested
Thickness	4.2 m	Tested
Gas content	22.4 m^3/t	Tested
Fracture length	140 m	Experience
Langmuir volume	30 m^3/t	Tested
Langmuir pressure	2.15 MPa	Tested
Reservoir pressure	6.0 MPa	Tested

net group in the study area are predicted using the COMET3 numerical simulation software.

5.1 Reservoir parameters

Reservoir parameters required in the simulation are shown in Table 3. It should be noted that before CBM drainage, the reservoir should be stimulated to improve the reservoir permeability. Based on actual permeability, permeability values of 0.01 mD, 0.05 mD, and 0.10 mD were set in this study.

5.2 Productivity prediction for a single well

Productivity prediction in 10 years for well ZD01 is shown in Figure 13. Under the three permeability values, the largest daily gas production is about 1,500–1,600 m^3/d. On day 250, the gas production reaches its peak value. The daily gas production is about 900–1,400 m^3/d on day 500, while it is about 600–1,000 m^3/d on day 1,000. The cumulative gas production is 1.7–3.2 × 10^6 m^3, with an average value of 2.4 × 10^6 m^3.

5.3 Productivity prediction for well net group

The well distance was set as 300 m. Production prediction in 10 years for a 5-well group was made using COMET3 software, and the results are shown in Figure 14. The maximum daily gas production of the well group is about 9,200–10,000 m^3/d. The

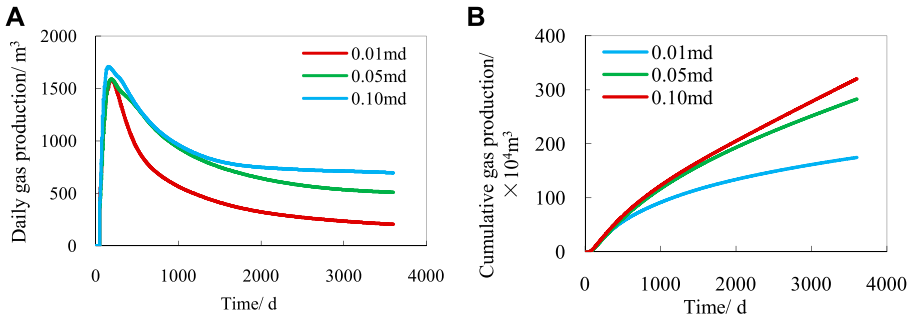

FIGURE 13
Daily **(A)** and cumulative **(B)** gas production for well ZD01.

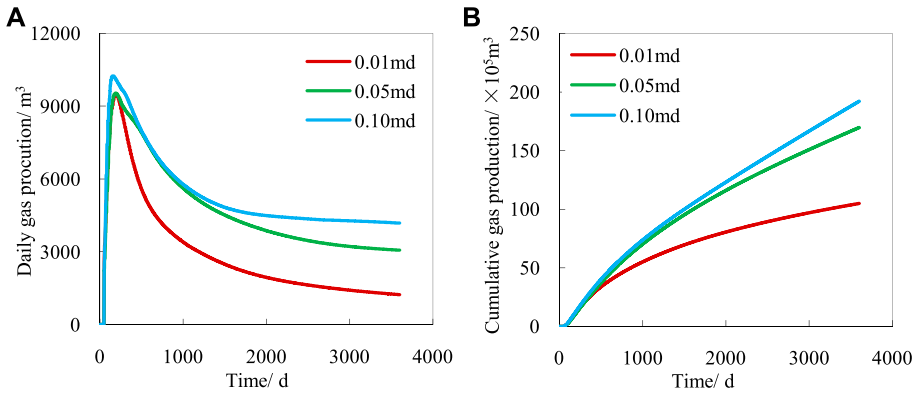

FIGURE 14
Daily **(A)** and cumulative **(B)** gas productions for a five-well group.

cumulative gas production in the first year is about 2.64×10^6 m^3, while it is 10.5–19.2 $\times$ 10^6 m^3 in 10 years, with an average of 14.5×10^6 m^3. Thus, it can be seen that there will be a high gas production in the study area after reservoir stimulation to obtain a good permeability.

6 Conclusion

The CBM geological occurrences of representative mining areas in the central Hunan depression were studied in this paper by measuring the maceral component, scanning electron microscope analysis, mercury intrusion porosimetry, permeability tests, isothermal adsorption measurements, well testing analysis, and gas content measurements. The drainage performance of a single well and a well group in the studied area were predicted using the numerical simulation method.

It was found that the vitrinite ranges from 54.37 to 87.80%, the inertinite is between 11.14 and 25.89%, and the exinite is less than 1%. The remaining 0.71–5.66% is an inorganic component, mainly clay mineral.

Most porosity is between 7 and 9%. The fitting analysis shows that the porosity negatively correlates with vitrinite content and positively correlates with inertinite content. Also, the porosity is negatively correlated with inorganic components and positively correlated with maximum vitrinite reflectance. Both the vertical and horizontal permeability are relatively low, with most values lower than 0.05 mD, indicating that the reservoir has low or no permeability.

Reservoir pressure ranges from 3.74 to 11.58 Mpa. The pressure has significant positive linear correlations with closure pressure and burial depth. Gas content varies mainly from 5 m^3/t to 20 m^3/t. The theoretical recoverability in the Hongshandian mining area is up to 61.7%, and the theoretical recovery in the two points of the Duanpoqiao mining area is 49.1 and 54.5%.

Numerical simulation results show that the cumulative gas production in 10 years for a single well is 1.7–3.2 $\times$ 10^6 m^3, and the productivity of a well net group consisting of five wells is 10.5–19.2 $\times$ 10^6 m^3 under permeabilities of 0.01 mD, 0.05 mD, and 0.10 mD.

Data availability statement

The original contributions presented in the study are included in the article/Supplementary Material; further inquiries can be directed to the corresponding author.

Author contributions

NC: laboratory experiments and data analysis; KW: paper writing; and JD: production perdition.

Acknowledgments

The authors wish to acknowledge the financial support for this study provided by the Scientific Research Project of the Natural Resource Department of Hunan Province under grant no. 2015-01.

Conflict of interest

The authors declare that the research was conducted in the absence of any commercial or financial relationships that could be construed as a potential conflict of interest.

Publisher's note

References

Bustin, R. M., and Clarkson, C. R. (1998). Geological controls on coalbed methane reservoir capacity and gas content. *Int. J. Coal Geol.* 38 (1-2), 3–26. doi:10.1016/s0166-5162(98)00030-5

Curtis, J. B. (2002). Fractured shale gas systems. *AAPG Bull.* 86 (11), 1921–1938. doi:10.1306/61EEDDBE-173E-11D7-8645000102C1865D

Huang, J. (1990). A further discussion of geochemical characteristics of natural gases in the Sichuan basin. *Geochimica* 3 (1), 307–321 [in Chinese with an English abstract]. doi:10.19700/j.0379-1726.1990.01.004

Laubach, S. E., and Gale, J. F. W. (2006). Obtaining fracture information for low permeability (tight) gas sandstones from sidewall cores. *J. Pet. Geol.* 29 (2), 147–158. doi:10.1111/j.1747-5457.2006.00147.x

Law, B. E. (2002). Basin-centered gas systems. *AAPG Bull.* 86 (11), 189–191. doi:10.1306/61EEDDB4-173E-11D7-8645000102C1865D

Law, B. E. (2002). Introduction to unconventional petroleum systems. *AAPG Bull.* 86 (11), 1851–1852. doi:10.1306/61EEDDA0-173E-11D7-8645000102C1865D

Li, Y., Wang, Y., Meng, S., Wu, X., Tao, C., and Xu, W. (2020). Theoretical basis and prospect of coal measure unconventional natural gas co-production. *J. China Coal Soc.* 45 (4), 1406–1418 [in Chinese with an English abstract]. doi:10.13225/j.cnki.jccs.2019.1305

Liu, X., and Wu, C. (2017). Simulation of dynamic changes of methane state based on NMR during coalbed methane output. *Fuel* 194, 188–194. doi:10.1016/j.fuel.2017.01.011

Liu, A., Fu, X., Wang, K., An, H., and Wang, G. (2013). Investigation of coalbed methane potential in low-rank coal reservoirs – free and soluble gas contents. *Fuel* 112, 14–22. doi:10.1016/j.fuel.2013.05.032

Martini, A. M., Walter, L. M., Ku, T. C., Budai, J. M., McIntosh, J. C., and Schoell, M. (2003). Microbial production and modification of gases in sedimentary basins: A geochemical case study from a devonian shale gas play, Michigan basin. *Am. Assoc. Pet. Geol. Bull.* 87 (8), 1355–1375. doi:10.1306/031903200184

Qin, Y. (2018). Research progress of symbiotic accumulation of coal measure gas in China. *Nat. Gas. Ind.* 38 (4), 26–36. doi:10.1016/j.ngib.2018.04.013

Schmoker, J. W. (1980). Organic content of Devonian shale in Western Appalachian basin. *AAPG Bull.* 64, 2156–2165. doi:10.1306/2F919756-16CE-11D7-8645000102C1865D

Sun, X., Zhang, Y., Li, K., and Gai, Z. (2016). A new mathematical simulation model for gas injection enhanced coalbed methane recovery. *Fuel* 183, 478–488. doi:10.1016/j.fuel.2016.06.082

Tao, S., Pan, Z., Tang, S., and Chen, S. (2019). Current status and geological conditions for the applicability of CBM drilling technologies in China: A review. *Int. J. Coal Geol.* 202, 95–108. doi:10.1016/j.coal.2018.11.020

Wang, B., Jiang, B., Liu, L., Zheng, G., Qin, Y., Wang, H., et al. (2009). Physical simulation of hydrodynamic conditions in high rank coalbed methane reservoir formation. *Min. Sci. Technol.* 19 (4), 435–440. doi:10.1016/s1674-5264(09)60081-8

Wei, Z. J., and Zhang, D. X. (2010). Coupled fluid flow and geomechanics for triple-porosity/dual permeability modeling of coalbed methane recovery. *Int. J. Rock Mech. Min. Sci.* 47 (8), 1242–1253. doi:10.1016/j.ijrmms.2010.08.020

Wei, C., Qin, Y., Wang, G. X., Fu, X., Jiang, B., and Zhang, Z. (2007). Simulation study on evolution of coalbed methane reservoir in Qinshui Basin, China. *Int. J. Coal Geol.* 72 (1), 53–69. doi:10.1016/j.coal.2006.12.001

Wei, C., Qin, Y., Wang, G., Fu, X., and Zhang, Z. (2010). Numerical simulation of coalbed methane generation, dissipation and retention in SE edge of Ordos Basin, China. *Int. J. Coal Geol.* 82 (3-4), 147–159. doi:10.1016/j.coal.2009.12.005

Zhang, J., and Bian, X. (2015). Numerical simulation of hydraulic fracturing coalbed methane reservoir with independent fracture grid. *Fuel* 143 (10), 543–546. doi:10.1016/j.fuel.2014.11.070

Zhang, J. (2014). Numerical simulation of hydraulic fracturing coalbed methane reservoir. *Fuel* 136, 57–61. doi:10.1016/j.fuel.2014.07.013

Zou, M., Wei, C., Fu, X., Bao, Y., and Cai, Z. (2013). Investigating reservoir pressure transmission for three types of coalbed methane reservoirs in the Qinshui Basin in Shan'xi Province, China. *Pet. Geosci.* 19, 375–383. doi:10.1144/petgeo2011-083

Zou, M., Wei, C., Yu, H., and Song, L. (2015). Modeling and application of coalbed methane recovery performance based on a triple porosity/dual permeability model. *J. Nat. Gas. Sci. Eng.* 22, 679–688. doi:10.1016/j.jngse.2015.01.019

Zou, M., Wei, S., Huang, Z., Lv, X., and Guo, B. (2018). Simulations on recoverability performances for a coalbed methane field in SE edge of Ordos basin, China. *Fuel* 233, 354–360. doi:10.1016/j.fuel.2018.06.071

Zou, C., Yang, Z., Huang, S., Ma, F., Sun, Q., Li, F., et al. (2019). Resource types, formation, distribution and prospects of coal-measure gas. *Petroleum Explor. Dev.* 46 (3), 451–462. doi:10.1016/s1876-3804(19)60026-1